A New Design Approach for Fiber DFB Lasers With Improved Efficiency

Kuthan Yelen, Louise M. B. Hickey, and Mikhail N. Zervas

***Abstract*—The standard distributed feedback (DFB) laser optimization method is critically investigated and a new design approach based on the effective cavity length is presented. By applying this method in an erbium–ytterbium co-doped fiber, the pump-to-signal conversion ratio is increased by 40% for the same total device length and pumping conditions. The laser with the proposed design is produced and the theoretical results are verified by the experimental work.**

***Index Terms*—Distributed feedback (DFB) lasers, erbium, gratings, optical fiber lasers, ytterbium.**

I. Introduction

DISTRIBUTED feedback (DFB) fiber lasers are attractive devices for a number of applications in the communications [1]–[3] and sensing [4]–[6] areas. A number of DFB fiber lasers can be configured in a parallel array to provide flexibility in pumping conditions and pump redundancy [7]. They can also provide stable single longitudinal mode and single polarization operation and the emitted wavelength can be set accurately with passive stabilization. They are inherently fiber compatible. In addition, they have low phase noise as well as low relative intensity noise (RIN). A number of different active dopants, such as erbium, ytterbium, neodymium, and thulium, can be used in order to cover different windows of the optical spectrum and offer extended coverage.

The overall optical efficiency is a key commercial driver as it minimizes the pump power required for either a single or multiplexed series of DFB fiber lasers. To date, efforts in improving DFB fiber laser efficiency have been based on *parametric* analysis. That is, certain parameters of the cavity such as grating length, grating strength, and position of the phase shift were varied over a range to find an optimum combination [8]–[11]. In this study, we present a new design approach that implements a simple apodization profile to enhance the position and length of the effective cavity without impacting the cavity asymmetry, cavity Q-factor, or the overall laser length. With the increased effective cavity length and increased delivered pump power, the optical efficiency increases. We explain how the effective cavity, in which the optical signal circulates, can be increased while maintaining the optimum reflectivities, so that a longer section of the active medium contributes to the signal generation. We discuss in detail a DFB fiber laser based on an erbium and ytterbium co-doped fiber. This combination of material is a well-known laser host, designed for high pump absorption around 975–980 nm and laser emission in the region 1528–1560 nm (telecommunication C-band). The design principles can be equally applied to other dopants and host materials as well as to semiconductor and planar DFB lasers.

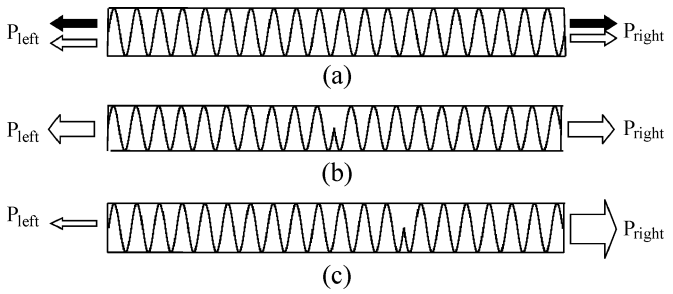

Fig. 1. Refractive index profile for conventional DFB laser designs. (a) Classic design and two-wavelength bidirectional operation. (b) Symmetric π-phase shifted design and single-wavelength bidirectional operation. (c) Asymmetric π-phase-shifted design and single-wavelength unidirectional operation.

II. Uniform Design

Traditionally, there have been three main DFB laser cavity designs that offer different performance and distinctive operational characteristics. A classic DFB laser, shown in Fig. 1(a), consists of a uniform refractive index grating, with constant amplitude and constant period, incorporated in an active medium. This type of DFB laser operates at two fundamental longitudinal modes at different wavelengths, corresponding to the edges of the grating bandgap, and gives symmetric output powers from both ends, P_{left} and P_{right}, which are equally divided between these two modes [12]. Such a cavity provides dual-wavelength bidirectional operation. In practice however, single-wavelength operation is desirable. This is achieved by introducing a π-shift in the spatial phase of the grating [13]–[15]. If the phase shift is located in the middle of the grating [Fig. 1(b)], due to the symmetry of the cavity, the output powers at both ends are equal. Such a cavity provides single-wavelength operation, coinciding with the grating Bragg wavelength, and bidirectional operation.

In addition to single-wavelength emission, unidirectionality is a very desirable feature of high-performance lasers. By placing the phase shift asymmetrically with respect to the grating center, as shown in Fig. 1(c), larger output power is obtained from the shorter end [10], [16]. In this asymmetric

Manuscript received December 22, 2003; revised February 26, 2004.

K. Yelen is with the Optoelectronics Research Centre (ORC), University of Southmapton, Southampton SO17 1BJ, U.K. (e-mail: ky@orc.soton.ac.uk).

L. M. B. Hickey is with Southampton Photonics, Inc. (SPI), Southampton SO30 2QU, U.K. (e-mail: louise.hickey@spioptics.com).

M. N. Zervas is with the Optoelectronics Research Centre (ORC), University of Southampton, Southampton SO17 1BJ, U.K., and is also with Southmapton Photonics, Inc. (SPI), Southampton SO30 2QU, U.K. (e-mail: mikhail.zervas@spioptics.com).

Digital Object Identifier 10.1109/JQE.2004.828257

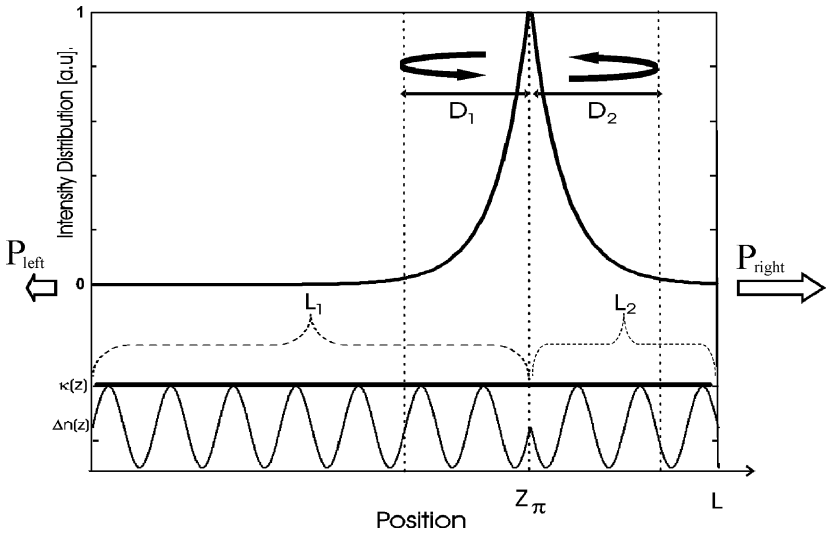

Fig. 2. Illustration of intensity distribution in a generic DFB laser with uniform $\kappa(z)$ and corresponding refractive index modulation $\Delta n(z)$. The phase of the grating is shifted by π at z_π. Seen from this position, there are two gratings in both directions of lengths L_1 and L_2. Fields propagating to the left and right, effectively, travel distances of D_1 and D_2, respectively.

design, the maximum output power from the desired end is obtained for a particular phase-shift position z_π and coupling coefficient value κ. Optimum values of parameters z_π and κ are found by varying them over a defined range, either by simulation or by experiment.

Fig. 2 illustrates the signal distribution inside a generic asymmetric DFB laser with uniform apodization profile. In this type of design, a very large intensity build up occurs around the phase shift. We think that the fields propagating to the left and to the right are trapped around the phase shift by the two grating segments and they are circulating within a short effective cavity. The peak signal intensity depends on the Q-factor of the effective cavity created by these two grating segments.

Each grating segment on either side of the phase shift can be considered as a separate reflector. The reflection coefficient r of a grating with constant gain at the Bragg wavelength is given by [17]

$$r = \frac{-\kappa \sinh(\gamma L)}{\gamma \cosh(\gamma L) - \alpha \sinh(\gamma L)} \tag{1}$$

where α is the field gain, κ is the coupling coefficient, L is the length of the grating, and $\gamma = \sqrt{\kappa^2 + \alpha^2}$. However, if α is small compared to κ, which is the case for most practical applications, then (1) can be simplified to

$$r \approx -\tanh(\kappa L); \quad \alpha \ll \kappa. \tag{2}$$

In our study, the maximum value of gain is around 3 m^{-1} and the typical coupling coefficient is 150 m^{-1}, so the approximation (2) holds. In this case, the reflectivity R of the grating is

$$R = |r|^2 \approx \tanh^2(\kappa L) \tag{3}$$

which is equal to the reflectivity of a passive grating with no gain.

Due to the distributed nature of the reflection process in gratings, the incident wave penetrates into the grating before reemerging at the front end. This effective distance is known as the penetration depth D, [18], which in the case of constant gain and at the Bragg wavelength is given by [19]

$$D = \frac{1}{2} \frac{\alpha L \left(\frac{\tanh(\gamma L)}{\gamma L} - \frac{1}{\cosh^2(\gamma L)} \right) + \tanh^2(\gamma L)}{\alpha \tanh^2(\gamma L) + \gamma \tanh(\gamma L)}. \tag{4}$$

However, if $\alpha \ll \kappa$, then D can be approximated by its passive cavity value

$$D \approx \frac{\tanh(\kappa L)}{2\kappa} = \frac{|r|}{2\kappa}. \tag{5}$$

In the case of a π-phase-shifted DFB laser, the total length of effective cavity L_{eff} in which the fields are circulating is

$$L_{\mathrm{eff}} = D_1 + D_2 \approx \left(\frac{|r_1|}{2\kappa_1} + \frac{|r_2|}{2\kappa_2} \right) \tag{6}$$

where D_1 and D_2 are the penetration depths into the grating segments on the left-hand side (l.h.s.) and on the right-hand side (r.h.s.) of the phase shift, respectively. In the case of a uniform refractive index profile, $\kappa_1 = \kappa_2 = \kappa$.

With the above definitions of reflectivity and effective cavity length, we can consider a closer look at the standard DFB output power optimization method. In our theoretical investigation we use the transfer-matrix method for the propagation of the fields [17] and the detailed gain medium model [20] with the excited-state absorptions and co-operative up-conversions of Er ions as well as the life-time quenching of Yb ions [21]. We first apply the parametric approach for the optimization of a 50-mm-long Er/Yb co-doped fiber DFB laser (see the Appendix for the used fiber parameters). We assume 200 mW of pump power at 978 nm is launched from the l.h.s. and we want to have maximum output power at 1552 nm coming out from the r.h.s. For different coupling coefficients κ, we vary the phase-shift position z_π and compute the laser output power characteristics. Fig. 3(a) shows the variation of the r.h.s. output power P_{right} with z_π for three different κ values. It is first shown that for each κ there is a different optimum phase-shift position that results in maximum output power from

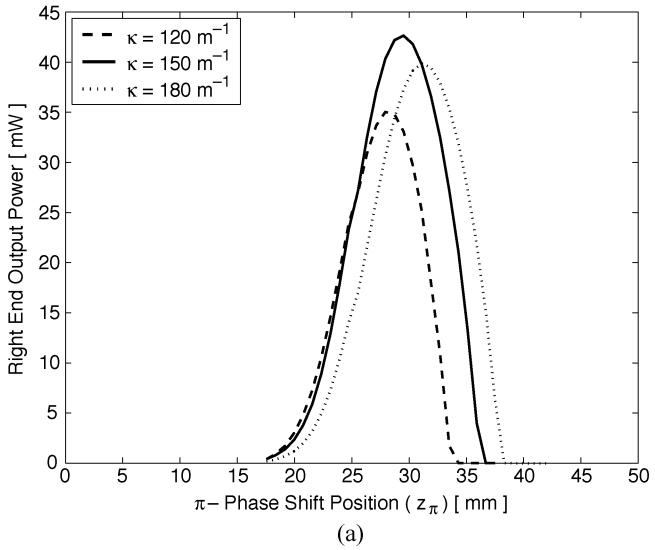

(a)

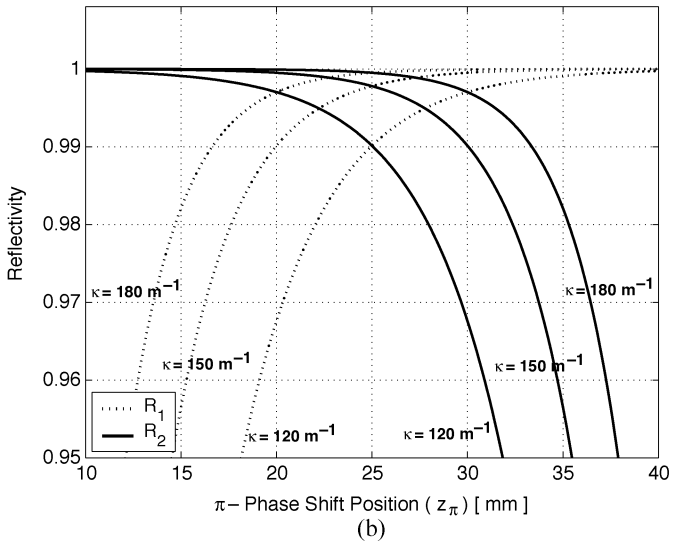

(b)

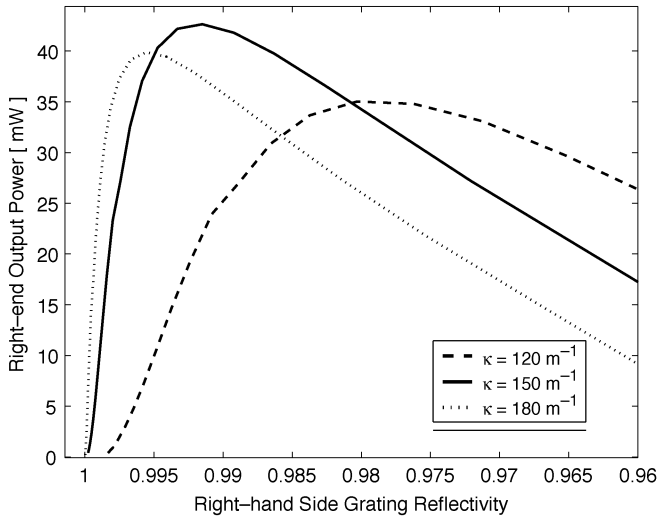

(c)

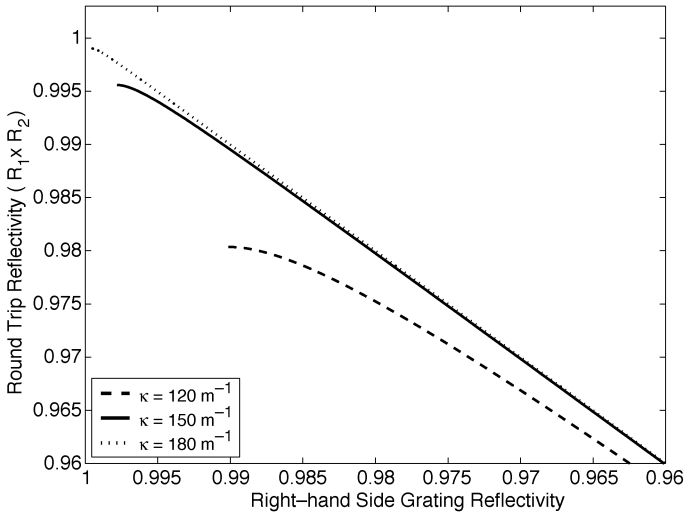

(d)

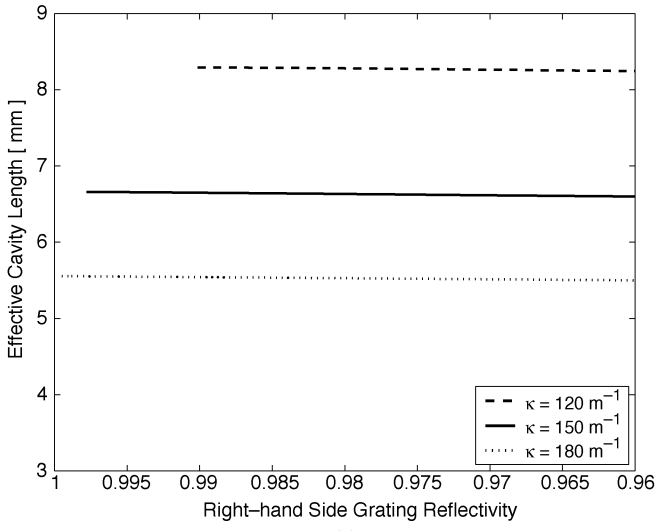

(e)

Fig. 3. (a) Variation of right-end output power ($P_{\rm right}$) with position of phase shift z_π in uniform DFB lasers. (b) Variation of reflectivities of gratings on the left (R_1) and right of the phase shift (R_2). (c) $P_{\rm right}$ variation as a function R_2. (d) Round-trip reflectivity $R_1 \times R_2$ as a function of R_2. (e) Comparison of effective cavity length for different κ as a function of R_2.

the desired end. The output power from the opposite end is about two orders of magnitude smaller resulting in almost perfect unidirectionality [16]. It is also evident that there is an optimum coupling constant κ that results in an overall maximum output power.

We should point out that, for each coupling constant, output power optimization in asymmetric DFB lasers is in essence similar to the Rigrod optimization of standard Fabry–Perot cavities [22], [23]. For each coupling constant, by moving the phase shift, we change the length of the l.h.s. grating L_1 and r.h.s. grating L_2, which leads to change in effective reflectivities R_1 and R_2, according to (3) as shown in Fig. 3(b). Therefore, we can rearrange the data of Fig. 3(a) to show explicitly the variation of P_{right} with the reflectivity of the r.h.s. grating R_2 as in Fig. 3(c). Here decreasing R_2 along the x axis corresponds to increasing z_π. Fig. 3(d) shows the variation in the round-trip reflectivity $R_1 \times R_2$ provided by the two gratings together, starting from the symmetrical cavity. The largest round-trip reflectivity, which is achieved when the phase shift is in the middle, for the weakest grating ($\kappa = 120\ \text{m}^{-1}$) is 0.98, indicating a rather weak cavity confinement. For the stronger gratings, however, this value can be very close to unity, showing a much stronger confinement. Fig. 3(e) shows the variation of the corresponding effective cavity lengths as a function of R_2. It is shown that increasing the grating coupling constant results in a decrease of the effective cavity length. On the other hand, the effective cavity remains greatly unaffected by the change of the phase-shift position.

The results of Fig. 3(c) and (e) make the equivalence to the Rigrod analysis quite obvious. Varying the DFB phase-shift position affects primarily R_2 and results in output power optimization, while the effective cavity remains practically constant. The existence of an optimum coupling constant (in this case $\kappa = 150\ \text{m}^{-1}$) can be understood by considering Fig. 3(d) and (e). Although smaller coupling constants (e.g. $\kappa = 120\ \text{m}^{-1}$) result in longer effective cavity [c.f. Fig. 3(e)], they show weaker cavity confinement [c.f. Fig. 3(d)]. For coupling constants higher then the optimum (e.g., $\kappa = 180\ \text{m}^{-1}$), the stronger cavity confinement is compromised by the decrease of the effective cavity length. This dependence is accentuated by the presence of the fiber background loss.

Now let's consider the case where z_π and κ have the optimum values. The largest output power is obtained when $z_\pi \approx 29$ mm (58% of total length) and $\kappa \approx 150\ \text{m}^{-1}$. The corresponding optimum reflectivities are $R_{1,\text{opt}} = 0.9993$ and $R_{2,\text{opt}} = 0.9927$. These values are in good agreement with literature on experimental and theoretical work using similar fibers and setups [10], [16]. Fig. 4 shows the average signal distribution (dashed line) at steady state inside the optimized design as well as the corresponding gain distribution (solid line). The main feature of the distribution is the building up of intensity to very large values around the phase shift. In this region, the active medium ions in the excited state undergo stimulated emission at a much higher rate due to the large signal intensity, causing the gain to drop substantially. In comparison, in the regions away from the phase-shift area, where the signal intensity, and, therefore, the stimulated emission is low, ions remain at the excited state and the gain remains close to the unsaturated value.

The value of L_{eff} in this optimum case is around 6.6 mm whereas the total device length is 50 mm, i.e., only a fraction of the available active medium interacts with the signal strongly. We propose that, by increasing the effective cavity length, we can utilize more of the active medium for signal generation, and therefore we can improve the laser output power without changing the total length of fiber or the pump power used.

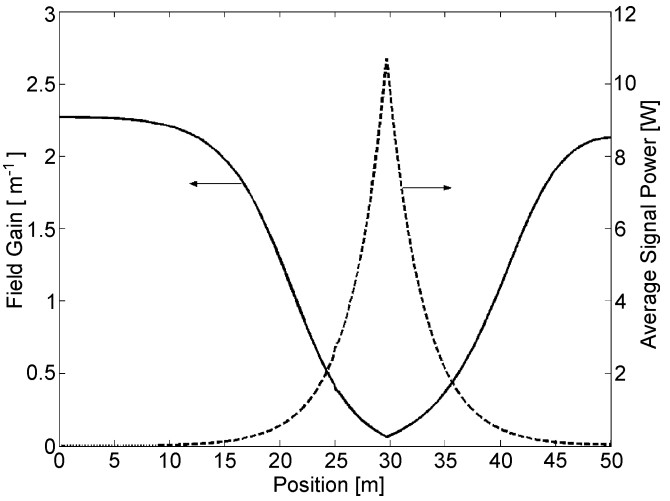

Fig. 4. Field gain and signal power distributions inside a 50-mm-long Er/Yb doped fiber at optimum $(\kappa, z\pi)$ pair. The intensity build up around phase-shift position $z\pi = 29$ mm causes gain to drop indicating power extraction from the medium but this build up quickly drops away from the phase shift, leaving large amount of gain outside the phase shift area.

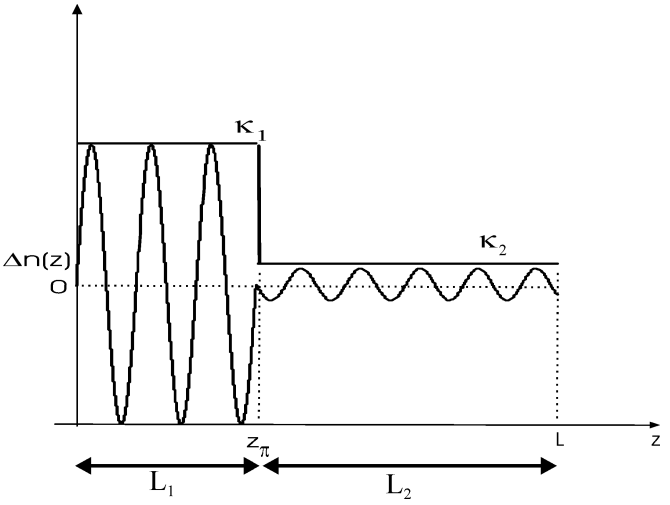

Fig. 5. Illustration of the step-apodized profile. As the phase shift is placed closer to the l.h.s., L_1 is reduced therefore larger κ_1 is required to keep R_1; however, L_2 increases, and therefore the κ_2 value is reduced.

III. Step-Apodized Design

One way of increasing the penetration depth, as (5) indicates, is to reduce the coupling coefficient. However, by doing so, we also reduce the reflectivity of the grating and, therefore decrease the optical feedback, and deviate from the optimum confinement condition. Considering (3), it is obvious that we can compensate for the reduction in the reflectivity due to smaller κ by increasing the segment length L. When the length of one of the segments is increased, the other segment's length must be decreased so that the total device length is not changed. With the same argument, in order to compensate for the reduced length of the other segment, its coupling coefficient must be increased so that the optimum reflectivity is restored. Such a DFB cavity is characterized by a step change in the coupling coefficient on either side of the phase shift. Fig. 5 shows a schematic of such a step-apodized DFB cavity.

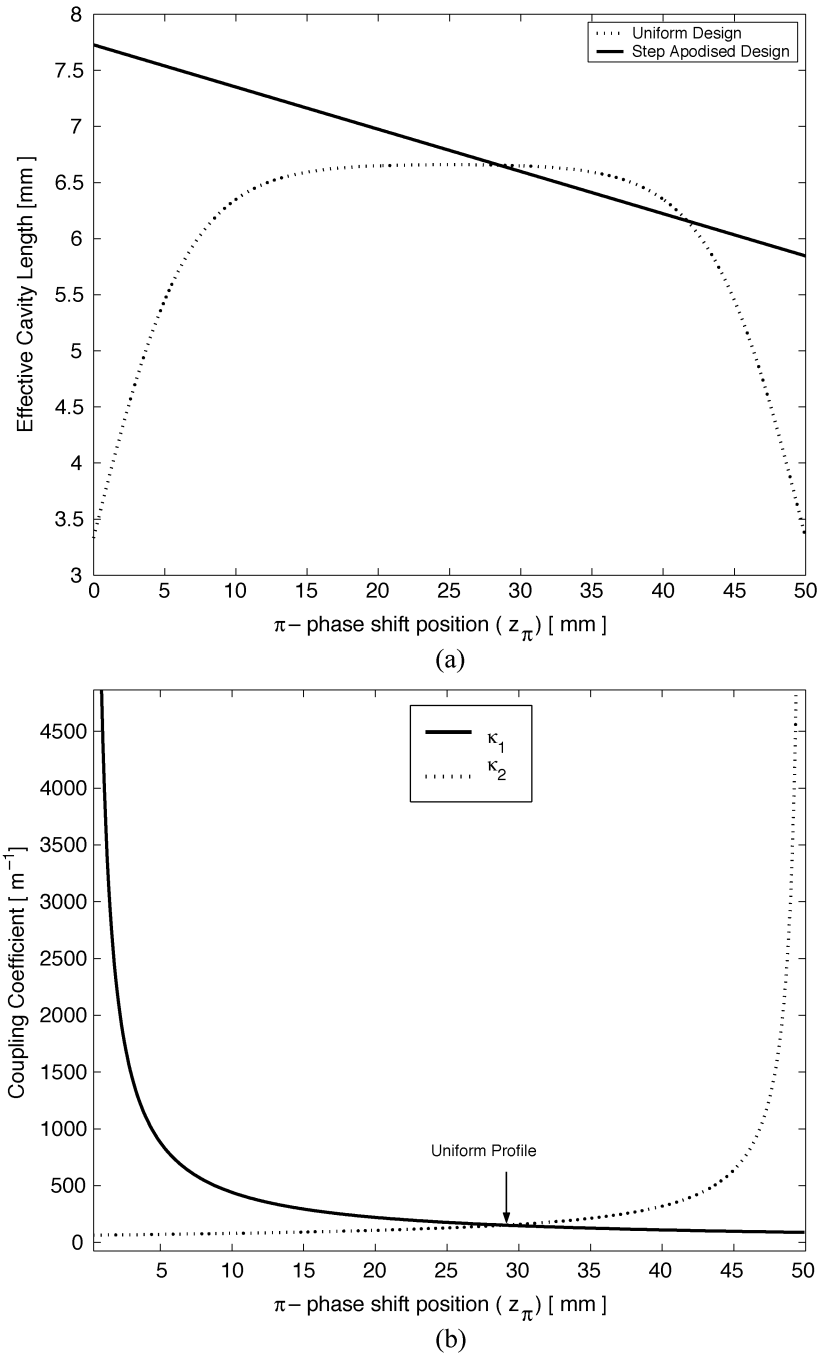

Fig. 6. (a) Variation of the effective cavity length $L_{\rm eff}$ with the phase-shift position. (b) Variation of the required coupling coefficients on both sides of the phase shift in order to keep the corresponding reflectivities fixed to their optimum values.

We can summarize the conditions that must be met as

$$\begin{aligned} \kappa_1 L_1 &= c_1 \\ \kappa_2 L_2 &= c_2 \\ L_1 + L_2 &= L \end{aligned} \tag{7}$$

where c_1 and c_2 are constants required to keep the reflectivies at the optimum values $R_{1,\rm opt}$ and $R_{2,\rm opt}$, respectively, and L is the total device length, which is also kept constant. Using (7) and setting $z_\pi = L_1$, we can rewrite (6) as

$$L_{\rm eff}(z_\pi) = \left[\frac{|r_2|L}{2c_2} + \left(\frac{|r_1|}{2c_1} - \frac{|r_2|}{2c_2}\right) z_\pi\right] \tag{8}$$

which is a linearly decreasing function of the phase-shift position as Fig. 6(a) shows (solid line). Compared with the effective cavity length variation in the optimum uniform-grating design (dotted line), the step-apodized profile increases $L_{\rm eff}$ significantly when the phase shift is moved toward the l.h.s. Fig. 6(b) shows the variation of the coupling coefficients of the grating segments on both sides of the phase shift. As the segment length gets smaller, a larger coupling coefficient is required to keep the reflectivity the same.

We again used the transfer-matrix method to simulate DFB lasers with a step apodization for different z_π positions. The total output power $P_{\rm Total}$ and $P_{\rm Right}$ show a linear variation with the position of phase shift, similar to the variation of the

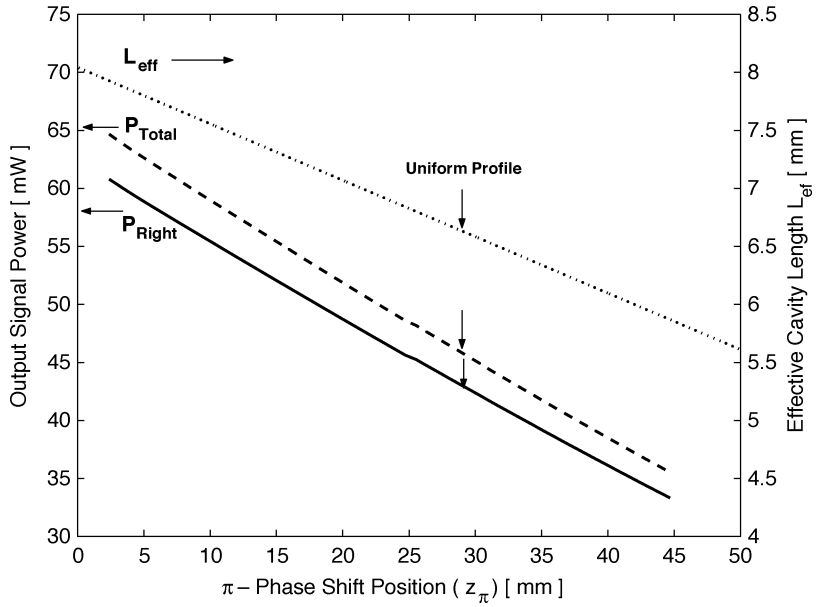

Fig. 7. Right end output power P_{Right} and total output power (left and right) P_{Total} variation with the position of phase shift in the step-apodized profile. Both show a linear variation with z_π, similar to L_{eff}, but have a different slope.

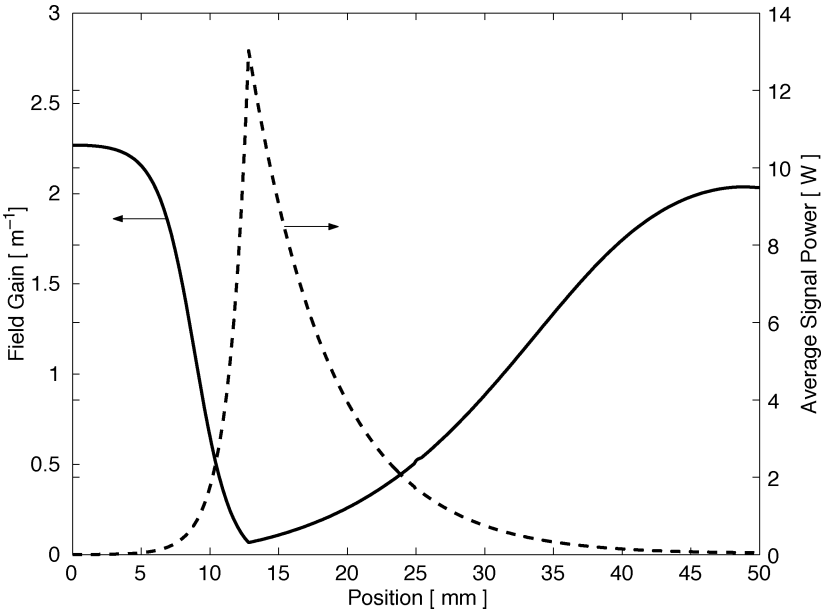

Fig. 8. Field gain and signal power distributions inside a 50-mm-long Er/Yb doped fiber with step apodization profile. The phase shift is placed at $z_\pi = 12.5\,\mathrm{mm}$.

effective cavity length. Fig. 7 shows the variation of effective cavity length as well as P_{Total}, and P_{Right} of a step-apodized DFB laser as a function of the phase-shift position. By placing the phase shift closer to the l.h.s., while preserving the optimum reflectivites, the total output power and r.h.s. output power can be increased up to 50% with respect to the optimum uniform profile values (indicated by the arrows). Cavities with similar designs having unity reflectors at one end have been reported earlier [13], [24], but the reason for such attempts was to attain single-sided output and not optimization of the efficiency.

As the phase shift is placed closer to the l.h.s., κ_1 must be increased to keep R_1 at the optimum level [see Fig. 6(b)]. In practice, the photosensitivity of the fiber will determine the maximum coupling coefficient that can be attained, which in turn will determine how short the l.h.s. segment can be. Coupling coefficients up to 500 m^{-1} are found to be feasible in the fibers we used. This value allows us to put the phase shift around 12.5 mm away from the l.h.s. end. Fig. 7 indicates that for maximum P_{right} the phase shift should be placed at $z_\pi = 0$. This is equivalent to a cavity comprised of a simple uniform grating butt-coupled to an external mirror or spliced to another passive grating of optimum reflectivity. In such a case, however, the nontrivial issue of introducing and maintaining the π phase shift should be addressed satisfactorily.

Fig. 8 shows the gain and average signal power distributions in a step-apodized cavity with z_π =12.5 mm. The effective cavity length in this case is 7.4 mm, corresponding to an increase of $\approx$12% with respect to the optimized uniform profile.

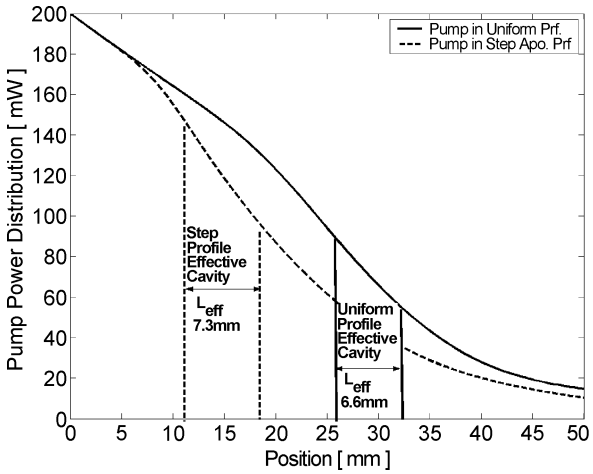

Fig. 9. Pump power distributions in DFB lasers with uniform profile (solid line) and step-apodized profile (dashed line). Effective cavities around the π-phase-shift regions are indicated with vertical lines.

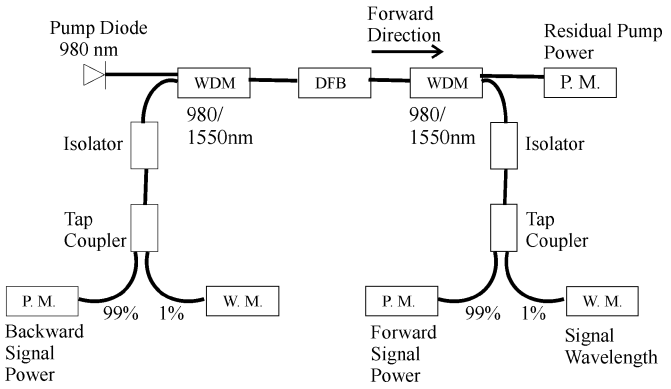

Fig. 10. Setup used to characterize DFB lasers.

The step-apodised profile not only increases the effective cavity length but also increases the pump power delivered into the effective cavity around z_π since in this case the phase-shift is placed closer to the pump source. Fig. 9 compares the pump power distributions in the optimized uniform and step-apodised profiles. The effective cavities of each profiles are also indicated in the Figure. In the step-apodised profile, the pump power delivered to the effective cavity is around 140 mW. In the uniform profile this value drops to 90 mW due to absorption by the longer segment between the pump source and the phase-shift region. With the combined effect of longer effective cavity and larger pump power, the pump-to-signal conversion increases from 22% to 27%.

IV. Experimental Results

We applied the step-apodized design approach experimentally in a Er–Yb codoped fiber. The fiber was produced using modified chemical vapor deposition (MCVD) technique [25]. The core of the fiber is a phosphosilicate host doped with Er, Yb, and Al. This active core is surrounded by a photosensitive germanosilicate ring doped with boron that matches the refractive index of the silica cladding. The core radius of the fiber is 2.3 μm and the cut-off wavelength is 1150 nm, giving $\mathrm{NA} = 0.1921$. The refractive index of the cladding (n_2) is 1.4585 and the corresponding core index (n_1) is 1.4709. In our simulations, we assume that the refractive index distribution is a step profile across the cross section of the fiber and we also assume that the dopants are uniformly distributed across the core. The refractive index grating is written in the photosensitive ring by exposing the fiber to ultraviolet (UV) interference pattern produced by a phase mask [26].

Fig. 10 shows the experimental setup used to characterize the DFB lasers. DFB lasers are pumped by a 980-nm semiconductor laser in a co-directional manner, that is, the pump power propagates in the same direction as the desired output end of the DFB laser. In this forward direction, a 980-nm/1550-nm wavelength-division multiplexing is used to separate the DFB output signal from the residual pump power. Residual pump power is measured by a power meter (PM). A tap coupler is used to feed 1% of the signal to a wave meter (WM) in order to measure the peak wavelength. The other arm of the coupler is connected to a PM to measure the output power in the forward direction. A similar setup is used on the other side of the DFB laser in order to measure the backward output power as well as the peak wavelength. On both sides, optical isolators prevent spurious back-reflections from entering and perturbing the DFB laser. The transmission of all components is measured, so that the output powers could be calculated from PM readings.

The semiconductor pump laser we used was electrically pumped and its output power is controlled by varying the drive current. Fig. 11(a) shows the relation between the drive current and the pump power delivered to the DFB laser after WDM.

The wavelength of the pump source is a defining factor in simulations since it affects the absorption by the active medium. It is especially critical if the pump operates between 970–980 nm where Yb cross sections change quite sharply with the wavelength [27], [28]. Over the tuning range of the pump diode, the spectrum peak shifts from 978 to 980 nm. We included this shift in our simulations by considering a linear variation in the pump wavelength, as shown in Fig. 11(b).

Using the uniform profile, first we experimentally determined the optimum coupling coefficient and phase-shift position for maximum P_{right} by producing a number of uniform DFB lasers with different strengths and different phase shift positions. The optimum value of κ and z_π were experimentally found to be 153 m^{-1} and 29 mm, respectively, for a 50-mm-long device. These experimental results are in very good agreement with the simulation results. Using these values we calculated the required step-apodized profile with the phase shift placed at z_π =12.5 mm, as discussed in the previous section, and, we fabricated a 50-mm-long DFB laser with the calculated step-apodized profile. Fig. 12 compares the theoretical and experimental values of the r.h.s. output power of uniform and step-apodized DFB lasers when the pump power is varied from 0 to 240 mW.

We found that theoretical and experimental results were in very good agreement for both lasers. Experimentally, the introduction of the step-apodised profile increased the laser output power from 42 mW to 56 mW, corresponding to increase in

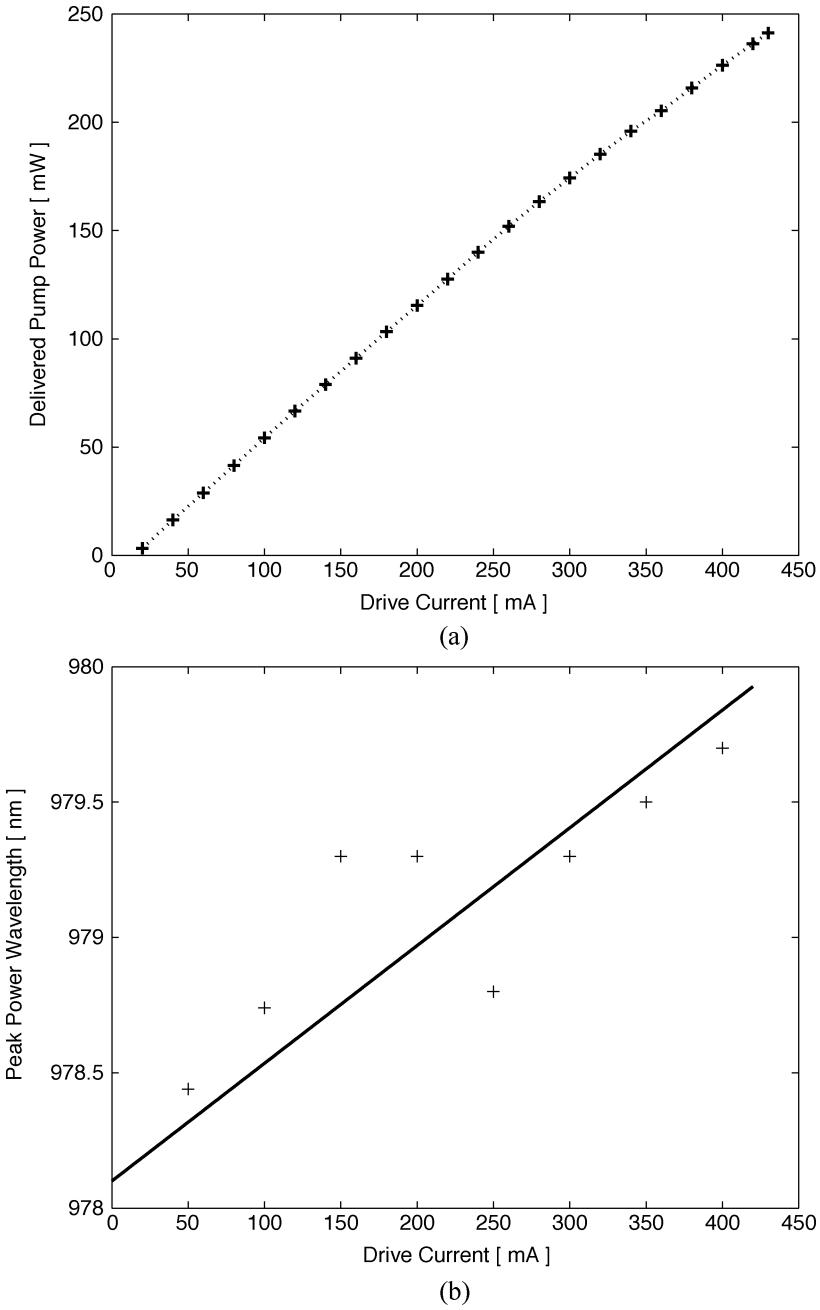

Fig. 11. Characteristics of the pump diode. (a) Drive current versus power delivered to the DFB laser. (b) Variation of the peak wavelength of the pump power with drive current. In the simulation, this variation is approximated by the solid straight line.

pump-to-signal conversion from 21% to 28%, both are very close to the values predicted by theory.

We believe the deviation between the simulations and the experiments at low pump powers may be due to a series of factors: The wavelength of the pump source abruptly changes with the drive current [see Fig. 11(b)], which is included in the simulation as only as a linear variation. Production of the devices requires splicing tolerances, which means there is a 4 ± 1-mm-long additional doped fiber before and after the grating. A 4-mm-long section is included in the model, but any error will impact the simulation especially at the low pump powers. Finally, heating and temperature distributions are known to affect the gratings in Er/Yb codoped fibers [29]. The phase shift could be approaching the ideal π value at the larger pump powers as a result of heating, whereas at low pump powers deviation from this value could lead to increased threshold values.

The step-apodized profile increases the pump power delivered to the effective cavity compared to the initial optimum uniform design (see Fig. 9), which means that the optimum values for the reflectivities can be slightly different. Therefore, additional optimization is possible by fine-tuning the position of phase shift around the step position. By doing so, we were able to increase the output power experimentally up to 60 mW for 200-mW pump power, increasing the pump-to-signal conversion to 30%.

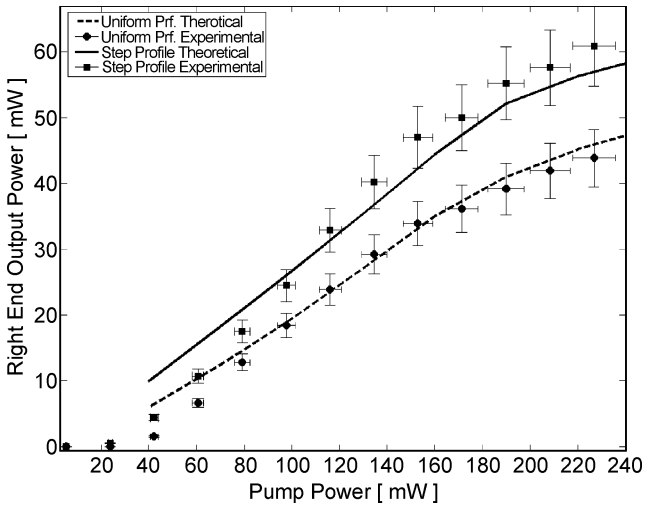

Fig. 12. Experimental and theoretical comparison of DFB lasers with uniform and step-apodized coupling coefficients. The phase-shift position in the step-apodized laser is placed at 12.5 mm due to practical limits in the maximum refractive index change that can be induced.

TABLE I
FIBER PARAMETERS USED IN THE SIMULATIONS

Parameter	*Value*
Pump Wavelength	**978 – 980 nm**
Yb Concentration	34×10^{25} m^{-3}
Yb pump absorption cross section	**$7.5 \times 10^{-25} - 4.4 \times 10^{-25}$ m^{-2}**
Yb pump emission cross section	$8.3 \times 10^{-25} - 5.9 \times 10^{-25}$ m^{-2}
Yb $^2F_{5/2}$ life-time	**2 ms**
Yb $^2F_{5/2}$ quenched life time	1 μs
Percentage of life-time quenched ions in total Yb concentration	**11%**
Signal Wavelength	1552 nm
Er Concentration	**3×10^{25} m^{-3}**
Er signal absorption cross section	1.4×10^{-25} m^{-2}
Er signal emission cross section	**2.5×10^{-25} m^{-2}**
$\sigma^{Er}_{p,a}$	3×10^{-25} m^{-2}
Er $^2I_{13/2}$ life-time	**10 ms**
Er $^2I_{11/2}$ life-time	0.6 μs
Er $^4F_{7/2}$, $^2H_{11/2}$, $^2S_{3/2}$ Non-radiative / radiative transition rate	**14×10^5 s^{-1}, 10^3 s^{-1}**
k_{tr}	8×10^{-22} m^{3}s^{-1}
$C_{up,2}$, $C_{up,3}$	**1×10^{-24} m^{3}s^{-1}**
$C_{ESA,2}$, $C_{ESA,3}$	1×10^{-27} m^{-2}
Signal Background Loss	**0.15 m^{-1}**
Core radius	2.3 μm
n1 , n2	**1.4709 , 1.4585**

V. CONCLUSION

Investigation of standard parametric optimization of π-phase-shifted DFB lasers has shown that the method is similar to the traditional Rigrod analysis of Fabry–Perot laser cavities. However, in the case of DFB lasers, the efficiency is also influenced by the effective cavity length, which in turn is determined by the grating coupling coefficient. Based on the last observation, we have developed a new way of optimizing DFB laser cavities. This method introduces a step-apodized profile that results in an increased effective cavity length without changing the reflectivities from their optimum values and without increasing the total grating length. In addition to longer effective cavity, this design increases the actual pump power delivered to the effective cavity since the phase-shift position is moved closer to the pump source.

We showed, both theoretically and experimentally, that in an Er/Yb doped fiber DFB laser this approach increased the pump-to-signal conversion from 21% to 28% as compared with an optimized uniform profile counter part. With further optimization of reflectivities for the larger pump power delivered, we increased this figure up to 30%. In implementing the step-apodized design, the photosensitivity of the fiber sets the practical limit. This method is not limited only to fiber DFB lasers, and it can be equally well applied to DFB laser devices in other rare-earth-doped fibers as well as in semiconductor and planar glass DFB lasers.

ACKNOWLEDGMENT

The authors gratefully acknowledge the SPI manufacturing staff for their help in the experimental verification of the theory. DFB laser production and characterization were carried out at the state-of-art facilities of SPI, Southampton, U.K.

REFERENCES

[1] J. Hubner, P. Varming, and M. Kristensen, "Five wavelength DFB fiber laser source for WDM systems," *Electron. Lett.*, vol. 33, no. 2, pp. 139–140, 1997.

[2] M. Ibsen, S. U. Alam, A. N. Zervas, A. B. Grudinin, and D. N. Payne, "8- and 16-channel all-fiber DFB laser WDM transmitters with integrated pump redundancy," *IEEE Photon. Technol. Lett.*, vol. 11, pp. 1114–1116, Sept. 1999.

[3] H. N. Poulsen, P. Varming, A. Buxens, A. T. Clausen, P. Munoz, P. Jeppesen, C. V. Poulsen, J. E. Pedersen, and L. Eskildsen, "1607 nm DFB fiber laser for optical communication in the L-band," presented at the ECOC, Nice, France, 1999.

[4] J. T. Kringlebotn, W. H. Loh, and R. I. Laming, "Polarimetric Er3+-doped fiber distributed-feedback laser sensor for differential pressure and force measurements," *Opt. Lett.*, vol. 21, no. 22, pp. 1869–1871, 1996.

[5] E. Ronnekleiv, M. Ibsen, and G. J. Cowle, "Polarization characteristics of fiber DFB lasers related to sensing applications," *IEEE J. Quantum Electron.*, vol. 36, pp. 656–664, June 2000.

[6] O. Hadeler, M. Ibsen, and M. N. Zervas, "Distributed-feedback fiber laser sensor for simultaneous strain and temperature measurements operating in the radio-frequency domain," *Appl. Opt.*, vol. 40, no. 19, pp. 3169–3175, 2001.

[7] L. B. Fu, M. Ibsen, J. K. Sahu, J. N. Jang, S. U. Alam, J. Nilsson, D. J. Richardson, D. N. Payne, C. Codemard, S. Goncharov, I. Zalevsky, and A. B. Grudinin, "Fiber-DFB laser array pumped with a single 1-W CW Yb-fiber laser," *IEEE Photon. Technol. Lett.*, vol. 15, pp. 655–657, May 2003.

[8] H. Soda, H. Ishikawa, and H. Imai, "Design of Dfb-lasers for high-power single-mode operation," *Electron. Lett.*, vol. 22, no. 20, pp. 1047–1049, 1986.

[9] J. E. A. Whiteaway, G. H. B. Thompson, A. J. Collar, and C. J. Armistead, "The design and assessment of lambda-4 phase-shifted DFB laser structures," *IEEE J. Quantum Electron.*, vol. 25, pp. 1261–1279, June 1989.

[10] V. C. Lauridsen, J. H. Povlsen, and P. Varming, "Design of DFB fiber lasers," *Electron. Lett.*, vol. 34, no. 21, pp. 2028–2030, 1998.

[11] ——, "Optimising Erbium-doped DFB fiber laser length with respect to maximum output power," *Electron. Lett.*, vol. 35, no. 4, pp. 300–302, 1999.

[12] H. Kogelnik and C. V. Shank, "Coupled-wave theory of distributed feedback lasers," *J. Appl. Phys.*, vol. 43, no. 5, pp. 2327–2335, 1972.
[13] J. T. Kringlebotn, J. L. Archambault, L. Reekie, and D. N. Payne, "Er3+Yb3+ codoped fiber distributed-feedback laser," *Opt. Lett.*, vol. 19, no. 24, pp. 2101–2103, 1994.
[14] W. H. Loh and R. I. Laming, "1.55 um phase-shifted distributed feedback fiber laser," *Electron. Lett.*, vol. 31, no. 17, pp. 1440–1442, 1995.
[15] M. Sejka, P. Varming, B. Hubner, and M. Kristensen, "Distributed feedback Er3+ doped fiber laser," *Electron. Lett.*, vol. 31, no. 17, pp. 1445–1446, 1995.
[16] M. Ibsen, E. Ronnekleiv, G. J. Cowle, M. O. Berendt, O. Hadeler, M. N. Zervas, and R. Laming, "Robust high power (>20 mW) all-fiber DFB lasers with unidirectional and truly single polarization outputs," presented at the CLEO, Baltimore, MD, 1999.
[17] M. Yamada and K. Sakuda, "Analysis of almost-periodic distributed feedback slab waveguides via a fundamental matrix approach," *Appl. Opt.*, vol. 26, no. 16, pp. 3474–3478, 1987.
[18] D. I. Babic and W. Corzine, "Analytic expressions for the reflection delay, penetration depth, and absorptance of quarter-wave dielectric mirrors," *IEEE J. Quantum Electron.*, vol. 28, pp. 514–524, Feb. 1992.
[19] F. Koyama, Y. Suematsu, S. Arai, and T. Tawee, "1.5–1.6 mu-m GaInAsP/InP Dynamic-single-mode (DSM) lasers with distributed Bragg reflector," *IEEE J. Quantum Electron.*, vol. QE-19, pp. 1042–1051, June 1983.
[20] F. Di Pasquale, "Modeling of highly-efficient grating-feedback and Fabry-Perot Er^{3+} Yb^{3+} co-doped fiber lasers," *IEEE J. Quantum Electron.*, vol. 32, pp. 326–332, Feb. 1996.
[21] R. Paschotta, J. Nilsson, P. R. Barber, J. E. Caplen, A. C. Tropper, and D. C. Hanna, "Lifetime quenching in Yb-doped fibers," *Opt. Commun.*, vol. 136, pp. 375–378, 1997.
[22] W. W. Rigrod, "Saturation effects in high-gain lasers," *J. Appl. Phys.*, vol. 36, no. 8, pp. 2487–2490, 1965.
[23] C. T. Meneely, "Laser mirror transmissivity optimization in high power optical cavities," *Appl. Opt.*, vol. 6, no. 8, pp. 1434–1436, 1967.
[24] W. H. Loh, L. Dong, and J. E. Caplen, "Single-sided output Sn/Er/Yb distributed feedback fiber laser," *Appl. Phys. Lett.*, vol. 69, no. 15, pp. 2151–2152, 1996.
[25] L. Dong, W. H. Loh, J. E. Caplen, J. D. Minelly, K. Hsu, and L. Reekie, "Efficient single-frequency fiber lasers with novel photosensitive Er/Yb optical fibers," *Opt. Lett.*, vol. 22, no. 10, pp. 694–696, 1997.
[26] A. Asseh, H. Storoy, B. E. Sahlgren, S. Sandgren, and R. A. H. Stubbe, "A writing technique for long fiber Bragg gratings with complex reflectivity profiles," *J. Lightwave Technol.*, vol. 15, pp. 1419–1423, Aug. 1997.
[27] H. M. Pask, R. J. Carman, D. C. Hanna, A. C. Tropper, C. J. Mackechnie, P. R. Barber, and J. M. Dawes, "Ytterbium-doped silica fiber lasers: versatile sources for the 1–1.2 um region," *IEEE J. Select. Topics Quantum Electron.*, vol. 1, pp. 2–13, Jan. 1995.
[28] X. Zou and H. Toratani, "Evaluation of spectroscopic properties of Yb3+-doped glasses," *Physical Review B*, vol. 52, no. 22, pp. 15889–15 897, 1995.
[29] Y. Z. Xu, H. Y. Tam, S. Y. Liu, and M. S. Demokan, "Pump-induced thermal effects in Er-Yb fiber grating DBR lasers," *IEEE Photon. Technol. Lett.*, vol. 10, pp. 1253–1255, Sept. 1998.

Kuthan Yelen was born in Edirne, Turkey, on June 27, 1977. He received the B.Sc. degree in electrical and electronics engineering from the Middle East Technical University (METU), Ankara, Turkey, in 1999 and the M.Sc. degree in optical fiber communications from the University of Southampton, Southampton, U.K., in 2001, where he is currently working toward the Ph.D. degree.

He has been participating in computational photonics activities including the characterization, modeling, simulation, and design of lasers, rare-earth-doped materials and gratings.

Mr. Yelen was the recipient of scholarships from the National Education Foundation (MEV) of Turkey between 1995 and 1999 and from the Turkish Education Foundation (TEV) between 1999 and 2000. He was a Chevening Scholar of the British Council during the same period. Between 2001–2004, he was the receipient of a research scholarship from the University of Southampton and the Overseas Research Students Award (ORS) from the Committee of Vice-Chancellors and Principals of the United Kingdom (CVCP).

Louise M. B. Hickey received the B.S. degree in physics from laser science and the Ph.D. degree from the University of Southampton, Southampton, U.K., in 1993 and 1998, respectively.

During her doctoral work, her main field of study was planar waveguides and lasers in Ti-diffused sapphire. From 1997 to 1999, she was awarded a Fellowship from the Royal Commission of the Exhibition of 1851 to continue her research into planar waveguide lasers at the Optoelectronics Research Centre, University of Southampton. Following a year with De Beers Industrial Diamonds, she joined Southampton Photonics Inc., Southampton, U.K., in 2001 and is currently working to extend the power and performance of in-fiber lasers.

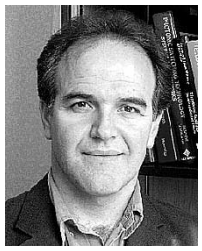

Mikhail N. Zervas was born on June 1, 1959 in Dimaina, Nafplion, Greece. He graduated from the University of Thessaloniki, Thessaloniki, Greece, in 1984, received the M.Sc. degree in applied and modern optics from the University of Reading, Reading, U.K., in 1985, and the Ph.D. degree in fiber optics from and University College London, London, U.K., in 1989.

He joined the Optoelectronics Research Centre, University of Southampton, Southampton, U.K., in 1991 as a Research Fellow and was promoted to Research Lecturer in 1995 and Professor of Optical Communications in 1999. His research activities include advanced optical fiber amplifier configurations, high-power fiber lasers, fiber DFB lasers, Bragg grating theory and devices, surface-plasmon effects and devices, optical trapping, and nano-particle manipulation. He is a co-founder of Southampton Photonics Inc., Southampton, where he is currently serving as Chief Scientist while on a university sabbatical leave. He has authored or coauthored over 170 technical publications and 25 patents/patent applications and has served on various conference program committees.

Prof. Zervas was the general program co-chair of the 1999 Optical Amplifiers Meeting (OSA) in Japan. He has given a number of invited talks and short courses in fiber gratings and fiber amplifiers at major international conferences. He was a coeditor of a Special Issue on Fiber Bragg Gratings of *Integrated and Fiber Optics*. In 1996, he was a co-recipient, with his colleagues, of the Metrology award from the Confederation of British Industry for their work on grating measuring systems for characterizing reflection and dispersion performance of fiber Bragg gratings.